AIAA JOURNAL
Vol. 40, No. 4, April 2002

Progress in Hypersonic Studies Using Electron-Beam-Excited X-Ray Detection

N. Gorchakova,* L. Kuznetsov,† and V. Yarygin‡
Institute of Thermophysics, 630090, Novosibirsk, Russia
B. Chanetz,§ T. Pot,¶ R. Bur,** J. P. Taran,†† and D. Pigache‡‡
ONERA, 92300 Châtillon, France
D. Schulte§§
DLR, German Aerospace Research Center, 51147 Cologne, Germany
and
J. Moss¶¶
NASA Langley Research Center, Hampton, Virginia 23681-2199

Experimental and numerical studies of the laminar shock-wave/boundary-layer interaction occurring past a hollow cylinder flare model in a Mach 10 air flow at zero incidence were conducted. Flowfield density measurements were performed by detecting x-ray emissions from the gas produced by electron-beam impact. A solution was found to make these measurements possible near the model surface. Wall pressure and heat flux measurements have been performed. All of the experimental results are compared with numerical results obtained by using Navier–Stokes and direct simulation Monte Carlo solvers.

Introduction

EXPERIMENTAL studies of the laminar shock-wave/boundary-layer interaction in rarefied hypersonic flows are delicate. Pressure taps and thermocouple elements can be mounted with some ease on the model surface, thus giving information at the model's boundary. However, the velocity, the density (or the pressure), and the static temperature of the flow near the model are hard to measure accurately and nonintrusively. Measuring is difficult largely because of the rarefied character of the flow. Yet the problem is of extreme interest, in the region where transition occurs between the continuum and the molecular regimes.

Viscous effects are of crucial importance in hypersonic flows because of the space occupied by the boundary layers. Shock-waves/boundary-layer interactions due to the impact of a shock-wave on a boundary layer can lead to overpressure and high-heat fluxes at the wall. The prediction of these effects is then necessary to design the control and the stability of hypersonic vehicles and their surface protection.

Electron-beam diagnostics now are well established for measuring the local parameters of rarefied gas flows (see Ref. 1 literature review). The gas parameters are determined from the radiation excited by an electron beam. The spectrum of the aforementioned radiation covers the range from the x-ray region to the visible. Ultraviolet and visible electron-beam-induced radiation is most generally employed for point density and temperature measurements, as well as for qualitative flow visualizations.[2–6] The fluorescence results from the formation of N_2^+ excited ions by the electron beam. The almost immediate drop of the ions to a lower energy state gives rise to a fluorescence whose intensity is roughly proportional to the density. However, quenching reduces fluorescence yield, and this method is not very quantitative above 10 Pa near room temperature. For quantitative point measurement of density at higher densities and temperatures, x-ray emission, composed of bremsstrahlung and characteristic radiation, is preferable because it is not subject to quenching and to spectral broadening. (Both depend on temperature and pressure and introduce nonlinearity in the response.) In principle, there are, thus, no physical limitations to employing this approach, provided the spatial resolution is much less than the electron mean free path.

The x-ray method of density measurements was proposed in Ref. 7 and fully implemented in Ref. 8. However, investigation of gas flows around models, particularly in the region close to their surface, is difficult with this technique. The reason is the interference of a strong x-ray radiation scattered from the surface when measurements are performed in the classical manner, namely, when the electron beam is positioned between the model and the x-ray detector, as shown in Fig. 1. It has been found that for usual electron-beam and flow parameters, the signal from the gas target is masked by this parasitic radiation near the model surface up to a distance of 15–20 mm. To limit this interference, a new method was proposed and implemented.[9] The electron beam is passed through a tube inserted into the model and cut flush at the model surface. The density measurements can then be made down to 2 mm from the surface.

In this paper, the x-ray technique is used to examine the airflow structure near a model specially designed for shock-wave/boundary-layer interaction studies. Undoubtedly, models with simple geometries are to be preferred for that purpose. Experiments over flat plates followed by ramps have been made for more than 25 years.[10,11] With these experiments, however, one could not achieve satisfactory two-dimensional flows because three-dimensional effects were observed when separation occurred. Inasmuch as a truly two-dimensional configuration is difficult to achieve in a hypersonic wind tunnel, because of the starting constraints that forbid the use of large spanwise models, it has been decided to perform a similar study on an axisymmetric configuration.

The model particulars and the measurement method are presented. Experimental density profiles were taken and compared with numerical simulations. Both continuum and Monte Carlo solvers

Received 11 March 2000; revision received 24 August 2000; accepted for publication 31 August 2001.

*Senior Scientist.
†Senior Scientist; deceased.
‡Team Research Leader.
§Head of Research Unit, Experimental/Fundamental Aerodynamics Department.
¶Research Engineer, Experimental/Fundamental Aerodynamics Department.
**Research Scientist, Experimental/Fundamental Aerodynamics Department. Member AIAA.
††Deputy General Scientific Director. Member AIAA.
‡‡Master of Research, Physics Department.
§§Research Engineer, Wind Tunnel Division, Institute for Fluid Mechanics.
¶¶Aerospace Engineer, Aerothermodynamics Branch, Aero and Gas Dynamics Division. Fellow AIAA.

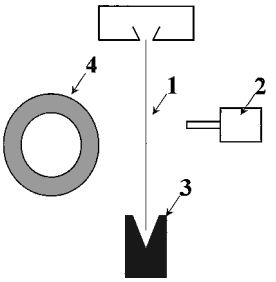

Fig. 1 Classical measurement approach: 1, electron beam; 2, Soller collimator and x-ray detector; 3, Faraday cup; and 4, model.

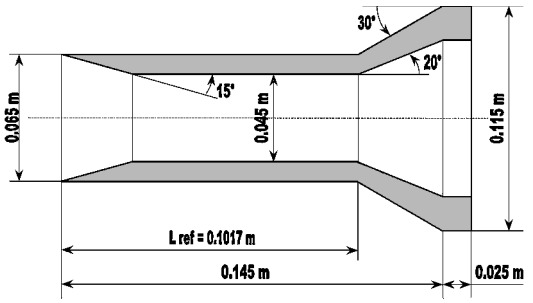

Fig. 2 Dimensions of model.

were used in generating the computed density profiles to compare with the measured data. The differences are discussed.

Facility and Model

Model and Surface Measurements

The model configuration is shown in Fig. 2. It is composed of a hollow cylinder with a sharp leading edge, followed by a flare terminated by a cylindrical extension. We take for reference the length $L = 0.1017$ m of the cylinder section. The wall pressure measurements have been executed with variable reluctance VALIDYNE™ DP 45 differential transducers. These transducers have been installed in the testing chamber and connected to the pressure taps by rubber tubes. For the measurement, a zero pressure reference, obtained by a turbomolecular pump, is applied to one side of the transducers. Wall pressure measurements are transformed into a pressure coefficient defined by

$$C_p = \frac{2(p/p_0 - 1)}{\gamma M_0^2}$$

where the freestream conditions M_0 and p_0 are deduced from the stagnation pressure measured with a pitot probe and from the reservoir pressure.

The heat fluxes are determined from the surface temperature rise (during the first seconds of the run) with a thermometer element (platinum film) that is applied to an insulating element made of ceramic. From the evolution of temperature with respect to time, heat flux is deduced for each sensor mounted on the model.

Experimental Procedure and Results

The experiments were carried out in the ONERA R5Ch wind tunnel. This tunnel provides a uniform Mach 10 air freestream environment with a density of about 4.3×10^{-4} kg/m^3. Flow visualization was accomplished by using the classical electron-beam-excited fluorescence in the visible and near UV (Ref. 12). The facility was also equipped with an electron-beam x-ray density measuring system.

For flow visualization the electron beam is swept in a raster mode at 50 Hz to create a visualization plane and the emitted light is photographed on film. Each photograph requires an exposure time of 10 s, which is sufficiently long to diminish (to average) the count fluctuation. With this method, shocks and flow nonuniformities are easily visualized.

The point density measurements needed for comparison with numerical code computations were performed as shown in Fig. 3 by using the electron gun in combination with x-ray measuring systems. The electron beam (25 keV and 0.8 mA) is here held fixed. It crosses the model between points c and d ensheathed through a thin-wall, stainless-steel tube of 2.8-mm i.d. and continues to the Faraday cup. The x-ray radiation at the point of measurement is selected by Soller collimators and detected with x-ray counters. The latter are equipped with preamplifiers. The signal is registered by a measuring unit BR-1. Detector six is mounted on a translation stage to measure the x-ray intensity along the d–e segment.

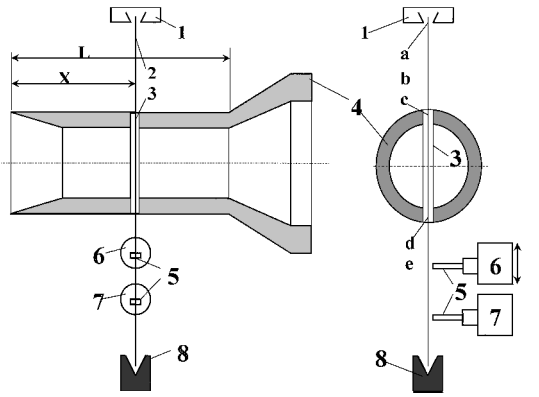

Fig. 3 Scheme of normal and axial cuts of the experimental facility (not to scale): 1, electron gun; 2, electron beam; 3, sheath tube; 4, model; 5, collimators; 6, and 7, detectors; and 8, Faraday cup.

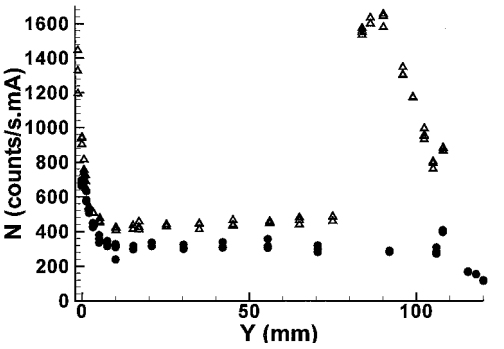

Fig. 4 Influence of the magnetic filter on detected x-ray counts at a static pressure of 150 mtorr: results ●, with and △, without magnetic filter.

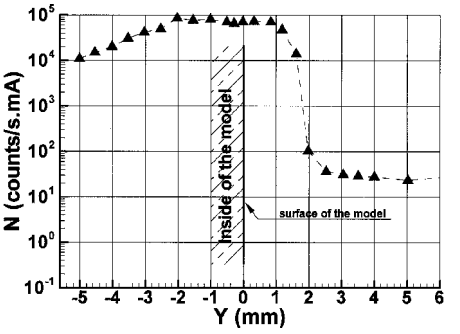

Fig. 5 Intensity profile of the parasitic emission near the model surface.

The Soller collimators are equipped with magnetic filters to prevent the penetration of scattered electrons. Tests have shown that these filters slightly diminish the penetration into the collimators of parasitic radiation from the model wall and significantly reduce that from the Faraday cup (Fig. 4). Y is the distance between the model surface and the measurement point. ($Y_0 = 0$ mm is on the model; $Y \approx 90$ mm is the Faraday cup upper surface.) Y_0 is the position for which the collimator axis is tangent to the cylinder. It is determined by two methods: 1) using the x-ray intensity profile under static conditions by moving the detector line of sight vertically with respect to the model (Fig. 5) and 2) using a thin tungsten wire placed under the beam, at a set distance from the model surface, and using the sharp response of the detector at this place (Fig. 6) as a marker of that distance.

The offset between the two calibration methods is about ± 0.3 mm. This is taken as our positioning accuracy. Figure 5 also shows that the

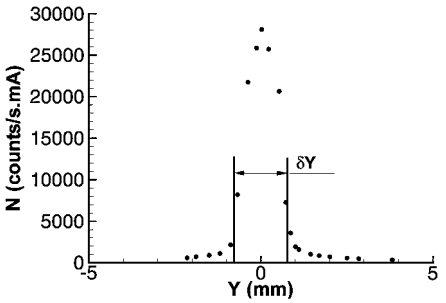

Fig. 6 Vertical spatial resolution of the Soller collimator.

closest distance at which accurate measurements are possible, on the cylindrical part, is equal to 2 mm. Moreover, N is not equal to zero in the region $Y < 0$ because the signal is not from the internal surface of the model but from the external one. The origin is the interaction of scattered electrons with the metal surface of model and its reflection. The quantity of scattered electrons is not much, but the intensity of radiation of electrons interacting with metal is much higher than during gas–electron interaction. It is also possible to determine the spatial resolution by moving the tungsten wire across the field of view of the collimator. The probe volume element is a segment of the electron-beam cylinder; its diameter is 1–2 mm (depending on the ambient pressure), and its height at half-maximum δY is found to be equal to a little less than 2 mm (Fig. 6), in accord with geometric predictions based on the collimator length (100 mm), its distance from the electron beam (160 mm), and the width of the collimator slit (0.45 mm).

The method of x-ray density measurement, described in Refs. 8 and 13, is based on that the integral intensity of x-ray radiation I is directly proportional to the gas number density n, namely,

$$I = cinz^2(V - V_d)/V$$

where z is the atomic number, c is a coefficient depending on the interaction cross section and detector aperture, and V and i are accelerating voltage and electron-beam current. The detector can be adjusted to detect only γ photons above a threshold energy V_d (in volts) and set in the soft x-ray region. This way, measuring absolute gas density can be accomplished by recording the x-ray radiation intensity I, normalized by electron-beam current i, as a function of gas density under static conditions: $I/i = f(n)$.

We work in the parameter range where the electron beam does not perturb the flowfield parameters; there is no electron-beam absorption influencing gas parameters. That is why we use the linear dependence, x-ray intensity vs density. The behavior of the calibration curves was investigated in special experiments where the electron beam current and accelerating voltage were changed over a rather wide range: current 0.1–3 mA and accelerating voltage 7.5–22.5 kV at density up to 10^{16} cm^{-3}, for N_2, O_2, He, and Ar. As a result, within these parameters, integral intensity of bremstrahlung x-ray radiation is directly proportional to the density and correspondent to the equation $I = cinz^2$.

When the flow is on, this calibration curve allows one to convert x-ray intensity measurements into gas density. Calibration, which reduces biases, also adds some uncertainties to the measurements. The error in the calibration is mostly due to the current measurement inaccuracy, which is itself caused by the electron-beam attenuation resulting from scattering via molecular collisions. The electron beam is scattered all along its path; thus, the current measured by the Faraday cup may not correspond to that at the point of measurement, but can be somewhat lower. This may introduce nonlinearity in the calibration curve $I/i = f(n)$ in the zones of high gas density. In practice, for the experimental conditions given in Ref. 9, the calibration curves (Fig. 7) covered the pressure range of 0–360 mtorr. In addition to the preceding error causes, there is a difference of electron-beam scattering under static conditions and in the flow. One possible way to extend the linear area of the calibration curve in the area of high gas density is to increase the accelerating voltage of the electron beam because beam scatter decreases with higher beam energy. However, it is not always technically possible.

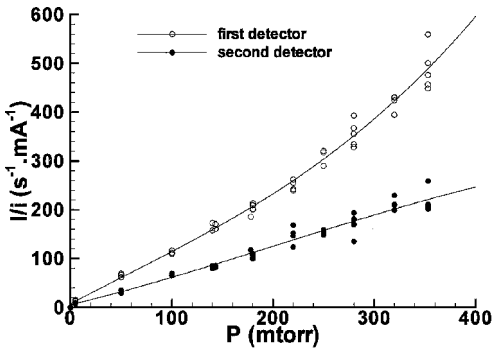

Fig. 7 Calibration curves of detectors.

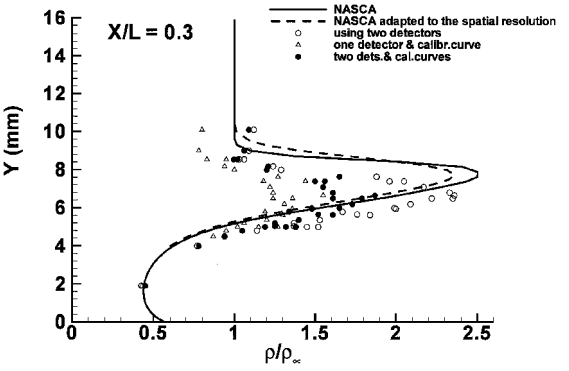

Fig. 8 Comparison between different measurement methods at X/L = 0.3.

Another option is to correct the calibration curve by using the calculated current values instead of the measured ones[14,15]; in this case, the result was based on measured current values and assumed flow properties. Unfortunately, this method does not give any definite answer concerning the error value. In view of the preceding difficulties, it was decided to implement a measurement scheme using two x-ray detectors, as shown in Fig. 3. Detector 6 is used to explore the shock and the boundary layer, whereas detector 7 remains trained on a fixed point in the freestream. The relative density maps ρ/ρ_∞ are, thus, obtained.

Figure 8, as an example, shows the radial density profile near the model for the cross section $X/L = 0.3$. The symbols are as follows: 1) Triangles represent the results obtained when using just detector 6 and a corresponding calibration curve (as an example, in Fig. 7 first detector) to get the absolute density values. 2) Filled circles represent the results obtained while measuring with detectors 6 and 7 but by using their calibration curves (see Fig. 7, first and second detector, respectively; I_1/i and I_2/i) to get the absolute density values ρ and ρ_∞. The difference between this curve and the preceding one reveals the influence of using measured values of ρ_∞ instead of calculated ones. This error is about 10–15% in the peak region. 3) Open circles represent the relative densities measured by detectors 6 and 7 using their intensity ratio only (without using calibration curves intensity vs density). 4) The dotted line represents the Navier–Stokes calculation (NASCA) results (see next section). 5) The dashed line is a modification of the NASCA computation degraded for the spatial resolution of the measurements by convoluting with the profile of Fig. 6.

Note that the only error source in the two-detector method is the determination of the intensity ratio of these two detectors under static conditions. To find this ratio, both detectors are aimed at the same measurement point, and their detected radiation intensities I_1 and I_2 measured. This intensity ratio gives the coefficient K from which one derives the relative density from the wind-on intensity ratio:

$$\rho/\rho_\infty = (1/K)(I_1/I_2)$$

Radial profiles of relative density also have been recorded successfully at other cross sections downstream and are presented later. However, difficulties were found at $X/L = 1.4$, for which higher

density prevails at the tube extremities and over a longer tube length. For these conditions, the electron-beam scattered so much when passing through the tube and shock layers that no more than 4% of the initial current reached the Faraday cup. Thus, the density measurements in the d–e region of Fig. 3 are impractical.

An alternative is to take measurements above the model in the b–c region by using the two-detector method. Thus, the tube inserted into the model serves as a sink to remove the electrons and to prevent them from scattering off the model surface. This method has been tested at $X/L = 0.76$. To verify the density measurements carried out above the model (b–c section), the behavior of x-ray radiation intensity along the electron-beam was investigated. As has been shown under static conditions, the intensity remains practically constant from a distance of 2 mm off the model wall. Furthermore, the results of wind-on relative density measurement were practically identical to those obtained previously below the model in the d–e region. This new procedure is made possible because of the magnetic filters that are placed at the entrance of the Soller collimators. Note that the method cannot be used for measuring the absolute density in the regions investigated; but only relative density measurements are feasible.

Numerical Calculation

Because of low pressures at high altitudes, the mean free path increases and may be of the magnitude of the body's reference length. The different domains of gasdynamics can be characterized by considering the Knudsen number Kn, which is equal to the ratio of the mean free path to the reference length L. In the R5Ch wind tunnel, the stagnation conditions are $p_0 = 250{,}000$ Pa, $T_0 = 1050$ K, and Knudsen number evaluated with the reference length $L = 0.1017$ m is equal to 0.005. Thus, the experiments have been performed in the continuum regime, and the use of the Navier–Stokes equations is justified. However, there are regions within the flow where the local Knudsen number is much larger than the global value, such as near the cylinder leading edge and within the shocks. Although they are primarily applied for the molecular regime, direct simulation Monte Carlo (DSMC) codes are also applicable in this domain. However, the density levels encountered of the R5Ch experiment requires a large number of cells, small time steps, and a large calculation time. Nevertheless, it is in this domain that it is possible to check both DSMC and Navier–Stokes solvers by comparison with the experiment.

NASCA Solver

The solver NASCA is based on a finite volume method for solving the classical Reynolds averaged Navier–Stokes equations. The problem investigated for this study is a steady one, thus allowing the use of the Beam-and-Warming-type time discretization,[16] which is first-order accurate in time. With regard to the space discretization, an implicit approach has been used. Acceleration techniques including alternate direction implicit factorization and local time stepping are used to speed up the convergence of the solution. The upwind scheme is an extension of the Osher and Chakravarthy[17] scheme to the case of a mesh which can be locally nonuniform and nonorthogonal (see in Ref. 18 for details). A classical central discretization is used for the viscous terms. For the present study, a 289×97 structured grid (axial times radial directions) was used.

FLOW Solver

The solver FLOW is based on a finite element method for solving the two-dimensional/axisymmetrical, unsteady, compressible Navier–Stokes equations. For a solution of these equations, a given computational domain has to be subdivided into cells, the so-called elements, where the governing equations are solved by an integral approximation.[19]

The applied numerical method uses an explicit Taylor–Galerkin algorithm in a weighted residual form, with a time integration according to the two-step version of the Lax–Wendroff scheme. For the prediction of steady-state solutions, local time step relaxation, in combination with a diagonalized, lumped mass matrix, is used. To improve shock capturing, especially with regard to high Mach numbers, the concept of flux-corrected transport (FCT) is applied to the Taylor–Galerkin algorithm. The principle of FCT can be characterized as a limitation of the antidiffusive fluxes of the Lax–Wendroff scheme, with the purpose of obtaining monotonic, first-order accurate solutions in the vicinity of shocks, while preserving the second-order accuracy in smooth regions of the flow.

When unstructured grids are employed, especially when using triangular elements, finite element methods permit a high level of geometric flexibility, enabling a detailed resolution of high-gradient variable regions.[20] The triangulation of the computational domain is accomplished by an automatic mesh-generation algorithm. To further improve the resolution of boundary layers, structured subgrids are employed at wall surfaces. For the present study, the computational domain is discretized by using a hybrid grid consisting of approximately 61,500 elements (after grid adaptation). The structured subgrid situated on the isothermal model wall is composed of 40 layers, growing with geometric progression.

DSMC Solver

The DSMC method provides a numerical capability that acknowledges the discrete nature of gas and thereby provides the capability of simulating flows across the complete flow spectrum of continuum to free molecular flow regimes. However, the computing requirements can become excessive for multidimensional continuum applications.

The molecular collisions are simulated by using the variable hard sphere (VHS) molecular model proposed by Bird.[21] This model employs the simple hard sphere, angular scattering law, so that all directions are equally possible for postcollision velocity in the center-of-mass frame of reference. However, the collision cross section is a function of the relative energy in the collision. Energy exchange between kinetic and internal modes is controlled by the Larsen–Borgnakke statistical model.[22]

For the present study, simulations are performed by using a nonreacting gas model consisting of two species, while considering energy exchange between translational, rotational and vibrational modes. A rotational relaxation collision number of 5 is used for the calculations. The vibrational collision number is 50. The calculations are made with a four-region computational domain containing 78,100 cells, where each cell is further subdivided into subcells (see Ref. 23 for details).

Results

General Structure of the Flowfield

Figure 9 shows the flow about the cylinder. It has been obtained with pure nitrogen to increase fluorescence. The attached shock-wave, at the sharp leading edge, and the separation shock-wave, formed upstream of the flare, are well visualized. These two shocks converge above the end of the flare.

The surface flow is shown by viscous coating visualizations. The pattern of the skin-friction lines is established during the run and identifies separated regions, showing their location and extent. The technique consists of projecting onto the model, before the test, a mixture of silicon oil, with a viscosity suited to the local skin-friction level, and markers. With such a mixture, we have visualized the separation line, located at $X/L = 0.76 \pm 0.01$, and the reattachment line, located at $X/L = 1.34 \pm 0.01$.

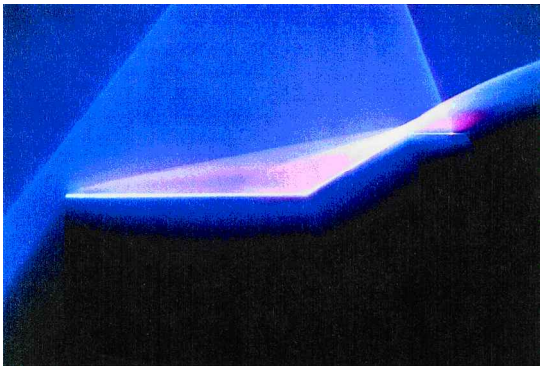

Fig. 9 Flowfield visualization by electron-beam fluorescence.

Table 1 Separation extent

Abscissa X/L	NASCA	FLOW	DMSC	Experiment
Separation	0.74	0.75	0.76	0.76 ± 0.01
Reattachment	1.33	1.33	1.32	1.34 ± 0.01

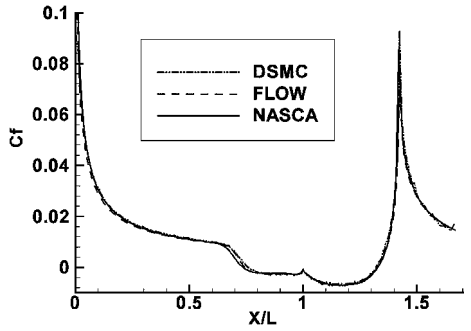

Fig. 10 Skin-friction coefficient distributions.

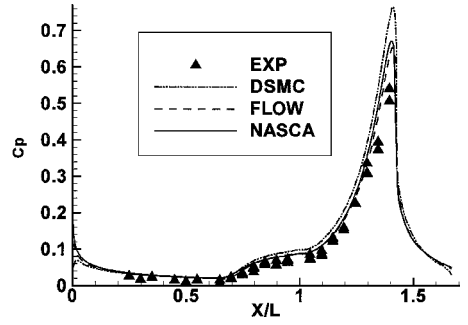

Fig. 11 Pressure coefficient distributions.

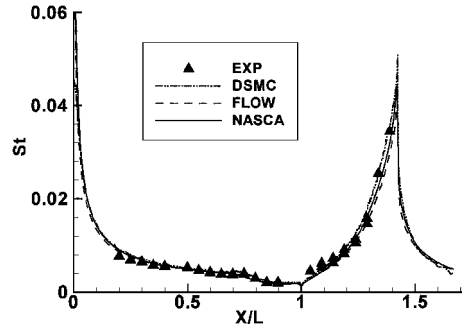

Fig. 12 Stanton number distributions.

Wall Results

The results obtained on the wall have already been compared to numerical results.[24] Spatial convergence is achieved by the three solvers, with the key parameters being the Stanton number and skin-friction coefficient evolutions. The skin-friction coefficient distributions (for which no experimental values have been measured) are shown in Fig. 10, which shows small differences in the prediction of the separation location as computed with the three different numerical solvers. In Table 1, the positions of the separation and attachment lines are reported; the measured values are inferred from flow visualizations as described in the preceding paragraph. The DSMC results show an exact prediction of the separation onset.

For the wall pressure distributions (Fig. 11), a comparison between the two Navier–Stokes solvers and the DSMC code reveals a good general agreement between calculations and the experiment (with an accuracy of measurement of $\pm 5\%$), especially for the separation prediction. However, there are some differences concerning the pressure level, which is overpredicted by calculations (already pointed out in Ref. 19). The source of the differences remains an open issue. Thus, some new pressure measurements must be performed to clarify the situation.

The heating rate comparisons given in Fig. 12 by the Stanton number distributions show good overall agreement. The distributions are characteristic of those for laminar flows, with the heating showing an initial decrease at the location of separation ($X/L = 0.76$), a cusp-like behavior at the cylinder/flare juncture, and a rapid increase along the flare. For this problem, the maximum heating rate occurs downstream of reattachment, which takes place just forward of the expansion onto the cylindrical extension.

External Flow Results

The measurements are performed using the electron-beam x-ray density system (described in the "Experimental Procedure and Results" subsection) with the two-detector method: one to measure the reference density in the freestream flow outside the boundary layer and the other to explore the boundary layer. Three density profiles have been obtained. The profile $X/L = 0.3$, shown in Fig. 13, is located forward of the separation line. At this station, the increase of density is due to the shock generated by the sharp leading edge. It is very satisfying to observe good agreement between numerical and experimental results for the density peak amplitude. However, the calculated radial shock position varies with the simulation used. At

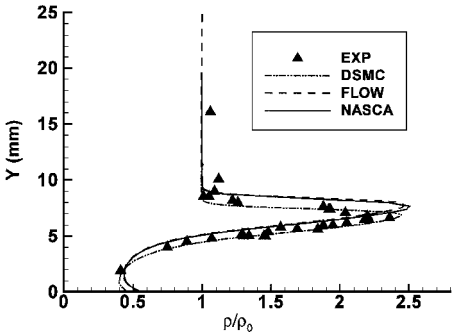

Fig. 13 Relative density at *X/L* = 0.30.

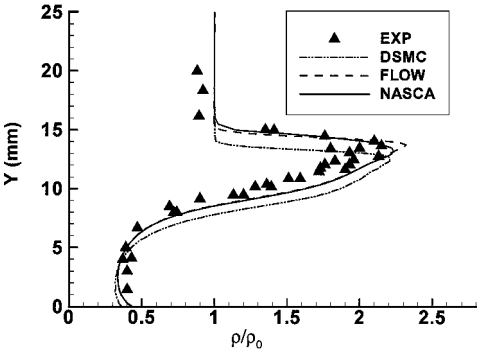

Fig. 14 Relative density at *X/L* = 0.60.

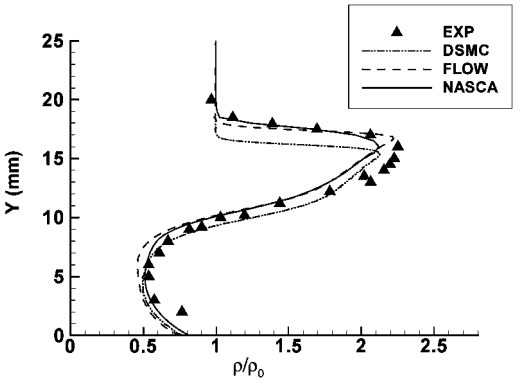

Fig. 15 Relative density at *X/L* = 0.76.

this station ($X/L = 0.3$), leading-edge effects probably remain an influence not accurately modeled by the Navier–Stokes solvers. That can be due to slip effects that are not taken into account and to the difficulty to keep the leading edge exactly with the mesh in Navier–Stokes approach. The DSMC calculation is in excellent agreement with the experiment. For the profiles at $X/L = 0.6$ (Fig. 14), the inverse phenomenon appears, that is, the better predictions are furnished by the two Navier–Stokes solvers. However, the difference between the radial shock locations needs to be confirmed before concluding this subject. The profiles at $X/L = 0.76$ (Fig. 15) present the same tendencies.

Conclusions

A new method for x-ray electron-beam gas-density measurements of the flow around an axisymmetrical model has been proposed and tested. By the use of this method, the density in the flowfield has been probed, thanks to an x-ray detection technique developed by the Thermophysics Institute of the Siberian Branch of the Russian Academy of Sciences in Novosibirsk. Measurements of gas density were successfully accomplished across shocks and boundary layers near a hollow cylinder with flare at cross sections $X/L = 0.3$, 0.6, and 0.76. The subject experiment, for validation of computational codes, constitutes a rare and valuable test case, in that it is entirely laminar without lateral effects. Therefore, it has been chosen for three different databases. Previously, it was a test case for AGARD Working Group 18. It has also been presented at the first Europe–U.S. High-Speed Flow-Field (HSFF) Database Workshop in Naples, Italy, held in November 1997, and it has been selected for presentation at the first Eastern-Western HSFF Database Workshop in Kyoto, Japan, in November 1998.

In this paper, three completely different solvers have been considered: a Navier–Stokes solver using a finite volume approach, a Navier–Stokes solver using the finite element method, and a DSMC solver using the VHS model. With regard to wall heat fluxes and density flowfield results, a good general agreement was found between calculations and experiment. Some discrepancies concerning the pressure results have been pointed out. A new pressure measurement campaign will be performed at ONERA to check the current results. The test will also include flowfield measurements based on dual lines coherent anti-Stokes Raman scattering for the determination of temperature, velocity, and density profiles.

Acknowledgments

The authors would like to thank F. Grasso from the University of Rome "La Sapienza" for providing the mesh used for Navier–Stokes calculations with the NASCA solver. They would also like to thank R. Benay from ONERA for providing the NASCA solver and J. Délery from ONERA for helpful discussions.

References

[1]Gochberg, L. A., "The Electron Beam Fluorescence in Hypersonic Aerothermodynamics," *Progress in Aerospace Sciences*, Vol. 33, 1997, pp. 431–480.

[2]Muntz, E. P., and Marsden, D. J., "Electron Excitation Applied to the Experimental Investigation of Rarefied Gas Flows," *Rarefied Gas Dynamics*, Vol. 2, Academic Press, New York, 1963, p. 495.

[3]Petrie, S. L., "Flow Field Analysis in a Low Density Arc-Heated Wind Tunnel," *Proceedings of the Heat Transfer and Fluid Mechanics Institute*, Stanford Univ. Press, Stanford, CA, 1965.

[4]Sebacher, D. J., "An Electron Beam Study of Vibrational and Rotational Relaxing Flows of Nitrogen and Air," *Proceedings of the Heat Transfer and Fluid Mechanics Institute*, Stanford Univ. Press, Stanford, CA, 1966.

[5]Bochkarev, A. A., Kosinov, V. A., Rebrov, A. K., and Sharafutdinov, R. G., "Measurement of Gas Flow Parameters Using an Electron Beam," *Experimental Methods in Rarefied Gas Dynamics*, Inst. of Thermophysics, Novosibirsk, Russia, 1974 (in Russian).

[6]Cattolica, R. J., Farley, D. R., and Clapp, L. H., "Electron Beam Dispersion in Carbon Dioxide," *Proceedings of the 21st International Symposium on Rarefied Gas Dynamics*, Vol. 2, edited by R. Brun, R. Campargue, R. Gatignol, and J. C. Lengrand, Cepadues Editions, Toulouse, France, 1998, pp. 567–574.

[7]Zigler, C. A., Bird, L. L., Olson, K. H., and Morreal, J. A., "Technique for Determining Density Distribution in Low Pressure," *High Temperature Gases, RSI*, Vol. 35, No. 4, 1964, pp. 450–456.

[8]Gorchakova, N. G., Kuznetsov, L. I., and Yarygin, V. N., "Electron Beam Diagnostics of High Temperature Rarefied Gas," *Proceedings of the 13th International Symposium on Rarefied Gas Dynamics*, Vol. 2, Plenum, New York, 1985, pp. 825–832.

[9]Bonnet, J., Chanetz, B., Henry, D., Larigaldie, S., Lefebvre, M., Mohammed, A. K., Pigache, D., Pot, T., Rosier, B., Taran, J. P., and Gorchakova, N., "Optical Diagnostics for Hypersonic Flows," *Proceedings of the International Conference on Methods of Aerophysical Research*, Vol. 1, ONERA, TP 1996-95, 1996, pp. 46–53.

[10]Holden, M. S., "A Study of Flow Separation in Regions of Shock-Wave/Boundary-Layer Interaction in Hypersonic Flow," AIAA Paper 78-1169, 1978.

[11]Délery, J., "Shock/Shock and Shock-Wave/Boundary Layer Interference Heating Analysis," *AGARD-FDP-VKI Special Course on Aerothermodynamics of Hypersonic Vehicles*, AGARD, 1988.

[12]Mohamed, A. K., Pot, T., and Chanetz, B., "Diagnostics by Electron Beam Fluorescence in Hypersonics," International Congress on Instrumentation in Aerospace Facilities Congress, ONERA, TP 1995-84, July 1995.

[13]Kuznetsov, L. I., Rebrov, A. K., and Yarygin, V. N., "Diagnostics of Ionized Gas by Electron Beam in X-ray Spectrum Range," *11th International Conference on Phenomena in Ionized Gases*, 1973.

[14]Sidelnikov, A. I., "Researching the New Opportunities of Measuring Gas Density Measurements by E-beam Method," *Journal of Applied Mechanics and Theoretical Physics*, No. 4, 1987, pp. 138–143 (in Russian).

[15]Mencher, Y. E., Palopezhentsev, S. A., and Yarygin, V. N., "About the E-beam Method of Gas Density Measurements," *Non-equilibrium Processes in Rarefied Gas Flows*, Inst. of Thermophysics, Novosibirk, Russia, 1977, pp. 108–112 (in Russian).

[16]Warming, R. F., and Beam, R. M., "On the Construction and Application of Implicit Factored Schemes for Conservation Laws," *SIAM-AMS Proceedings*, Vol. 11, 1978.

[17]Osher, S., and Chakravarthy, S., "Very High Order Accurate TVD Schemes," NASA Rept. 84-44, 1984.

[18]Benay, R., and Servel, P., "Applications of a Navier–Stokes Code to the Calculation of Missile or Aircraft Afterbody Flows," *Aerospace Research*, No. 1995-6, 1995, pp. 405–426.

[19]Koschel, W., Rick, W., and Rüggeberg, T., "Study of Flow Phenomena in High Speed Intakes," AIAA Paper 92-5029, 1992.

[20]Schulte, D., Henckels, A., and Wepler, U., "Reduction of Shock Induced Boundary Layer Separation in Hypersonic Inlets Using Bleed," *Aerospace Science and Technology*, Vol. 2, No. 4, 1998, pp. 231–239.

[21]Bird, G. A., *Molecular Gas Dynamics and the Direct Simulation of Gas Flows*, Clarendon, Oxford, 1994.

[22]Borgnakke, C., and Larsen, P. S., "Statistical Collision Model for Monte-Carlo Simulation of Polyatomic Gas Mixtures," *Journal of Computational Physics*, Vol. 18, No. 4, 1975, pp. 405–420.

[23]Moss, J. N., Olejniczak, J., Chanetz, B., and Pot, T., "Hypersonic Separated Flows at Low Reynolds Number Conditions," *Proceedings of the 21st International Symposium on Rarefied Gas Dynamics*, edited by R. Brun, R. Campargue, R. Gatignol and J. C. Lengrand, Vol. 2, Cepadues Editions, Toulouse, France, 1998, pp. 617–624.

[24]Chanetz, B., Benay, R., Bousquet, J. M., Bur, R., Pot, T., Grasso, F., and Moss, J., "Experimental and Numerical Study of the Laminar Separation in Hypersonic Flow," *Aerospace Science and Technology*, No. 3, 1998, pp. 205–218.

R. P. Lucht
Associate Editor